Published by Nigerian Society of Physical Sciences. Hosted by FLAYOO Publishing House LTD

Proceedings of the Nigerian Society of Physical Sciences

Journal Homepage: https://flayoophl.com/journals/index.php/pnspsc

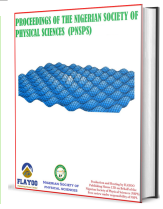

Measurement of dielectric properties of prepared stable nanofluids using coated TiO_2 nanoparticle-based palm kernel oil

Muhammad Ya'u Muhammad[a,*], Abdelghaffar Amoka Abdelmalik[b], Yusuf Musa Abubakar[b], Abubakar Ibrahim Balarabe[c]

[a] *Electrical Engineering Department, Jigawa State Polytechnic for Information and Communication Technology, Kazaure, Jigawa State, Nigeria*
[b] *Department of Physics, Ahmadu Bello University, Zaria, Kaduna State, Nigeria*
[c] *Department of Physics, Jigawa State College of Education, Gumel, Jigawa State, Nigeria*

ABSTRACT

Demand for environmentally friendly, high-performance insulating fluids has increased interest in bio-based nanofluids with improved dielectric behaviour. This study measures and analyses stable nanofluids prepared by dispersing oleic-acid-coated titanium dioxide (TiO_2) nanoparticles in methyl ester obtained from palm kernel oil. Fourier-transform infrared (FTIR) spectroscopy was used to characterise the coated nanoparticles, and nanofluids were prepared at controlled concentrations using mixing and stabilisation procedures. The samples were assessed for viscosity, pour point, flash point, relative permittivity, loss factor, leakage current, and direct-current (DC) and alternating-current (AC) breakdown strength. Dielectric measurements were carried out over 20–200 kHz using a Rohde & Schwarz HM8118 programmable inductive-capacitive-reactance bridge. The results show that oleic-acid coating improved nanoparticle dispersion stability, while increasing nanoparticle concentration enhanced dielectric performance. Among the tested samples, ECNF0.6 gave the best insulating response. The findings indicate that TiO_2-based palm kernel oil nanofluids are promising sustainable insulating materials for oil-filled electrical power equipment.

Keywords: Insulating fluids, Dielectric properties, TiO_2 nanoparticles, Nanofluid stability.

DOI:10.61298/pnspsc.2026.3.321

1. INTRODUCTION

Nanofluids, engineered colloidal suspensions of nanoparticles in base fluids, have emerged as advanced working fluids in thermal and electrical applications because of their enhanced physico-chemical properties compared with conventional fluids. Since the seminal work by Choi [1], who first introduced the term nanofluid, research has focused on how nanoparticles influence heat transfer, rheology and electrophysical behaviour in base fluids. Nanofluids containing metal oxides such as titanium dioxide (TiO_2) have attracted particular interest because of their chemical stability, nontoxicity, high dielectric constant and excellent dispersion characteristics in various media [2].

The dielectric properties of nanofluids, quantified by parameters such as dielectric constant, dielectric loss and electrical conductivity, are critical in applications such as high-voltage insulation, microelectronic cooling and capacitive energy storage. These properties not only influence the interaction of the fluid with electric fields but also reflect the underlying dynam-

*Corresponding Author Tel. No.: +234-703-6176-088.
e-mail: myfandum@gmail.com (Muhammad Ya'u Muhammad)

ics of nanoparticle–base-fluid interfaces and charge-transport mechanisms [3]. Dielectric behaviour in nanofluids can deviate significantly from that of the pure base fluid because of Maxwell–Wagner–Sillars polarisation, interfacial-layer formation and nanoparticle-charging effects [4].

Palm kernel oil (PKO), a biodegradable and sustainable vegetable oil, has been proposed as an eco-friendly base fluid for advanced nanofluids. Its relatively high intrinsic dielectric constant and thermal stability make it suitable for high-voltage electrical systems and thermal-management applications. However, the dispersion stability of nanoparticles in nonpolar vegetable oils remains a major challenge because of strong particle aggregation driven by van der Waals forces. Surface modification of nanoparticles through coating, for example with surfactants or insulating shells, is therefore essential to achieve long-term stability, reduce sedimentation and tailor interfacial properties [5].

Among potential nanoparticles, TiO_2 is widely used owing to its high relative permittivity, chemical inertness and ease of surface functionalisation. Coated TiO_2 nanoparticles, in which a dielectric or surfactant layer is grafted onto the particle surface, have been shown to exhibit enhanced dispersion and controlled electrical interactions in oil-based fluids [6, 7]. The coating can influence the effective dielectric constant of the nanofluid by modifying interfacial polarisation and inhibiting particle clustering, which is a key factor affecting dielectric relaxation and AC conductivity responses [8].

The objective of this study is to systematically measure and analyse the dielectric properties of stable nanofluids prepared by dispersing coated TiO_2 nanoparticles in palm kernel oil. Dielectric measurements under varying frequencies and temperatures are used to elucidate complex permittivity behaviour and provide insights into polarisation mechanisms and charge-transport phenomena in these nanofluids. Understanding the interplay among nanoparticle coating, concentration and base-fluid characteristics is expected to support the design of next-generation insulating fluids for power systems and advanced cooling technologies.

2. THEORETICAL BACKGROUND

2.1. RELATIVE PERMITTIVITY

Relative permittivity (ε_r) characterises how a material behaves in an electric field. It indicates how easily the electrical response of a liquid dielectric can change when an electric field is applied [9]. The ratio of absolute permittivity (ε) to the permittivity of free space (ε_0) is known as relative permittivity. Consequently, a high relative permittivity is required for a suitable insulating fluid [10]:

$$\varepsilon_r = \frac{\varepsilon}{\varepsilon_0}. \tag{1}$$

2.2. DIELECTRIC POLARISATION

Polarisation can cause positive charges to be displaced toward the field, while negative charges shift in the opposite direction. When an insulator is present in an electric field, electrical charges do not travel through the material, unlike in a conducting material [11]. The dipole moment (μ) of a dielectric is the product of charge (q) and the displacement between the two charges (d):

$$\mu = qd. \tag{2}$$

The electric displacement is expressed as

$$D = \varepsilon E, \tag{3}$$

where E is the applied electric field.

Materials with high permittivity polarise more strongly in response to an applied electric field and have greater energy-storage capacity. Dielectric polarisation P is the vector sum of the induced dipole moment and is directly proportional to the strength of the electric field:

$$P = \varepsilon_0 \alpha E. \tag{4}$$

Here, α is the polarisability of the molecules, with $\mu = \alpha E$, and ε_0 is the permittivity of free space (8.85×10^{-12} F m^{-1}). There are four mechanisms of dielectric polarisation.

Electronic polarisation occurs in a neutral atom and arises from displacement of the positively charged nucleus and the negatively charged electrons in opposite directions when an electric field is applied. This creates a dipole moment in a dielectric material. It is exhibited by monoatomic gases and is proportional to the volume of atoms and independent of temperature. The electronic polarisability, α_e, is

$$\alpha_e = 4\pi\varepsilon_0 R^3, \tag{5}$$

where R is the radius of the atom.

Ionic polarisation occurs when negative and positive ions are displaced in opposite directions when an electric field is applied. It occurs only in ionic solids, and the displacement is independent of temperature:

$$\alpha_i = \frac{e^2}{\omega_0^2}\left(\frac{1}{m} + \frac{1}{M}\right), \tag{6}$$

where e is the electron charge, ω_0 is the angular frequency, m is the mass of the positive ion and M is the mass of the negative ion.

Orientation polarisation is the main polarisation mechanism in liquids. It occurs in polar molecules with permanent dipole moments even in the absence of an electric field. When this material is kept in an electric field, the molecules align along the field direction, resulting in a dipole moment in the field direction. Orientation polarisation, P_o, is given by

$$P_o = \frac{N\mu^2 E}{3k_B T} = N\alpha_o E, \tag{7}$$

where

$$\alpha_o = \frac{\mu^2}{3k_B T}. \tag{8}$$

Space-charge polarisation occurs in heterogeneous dielectrics, such as partially crystalline insulating materials, which have positive and negative ions as free charge carriers. Without an external field, the dielectric is neutral and the positive and negative charges neutralise each other. Under an external electric field, the charge carriers in the dielectric move toward oppositely polarised electrode surfaces, giving rise to a macroscopic dipole. When the applied electric field is removed, the dielectric returns to its original neutral state. Dielectrics with this type of polarisation mechanism are also described as nonpolar, because they do not build

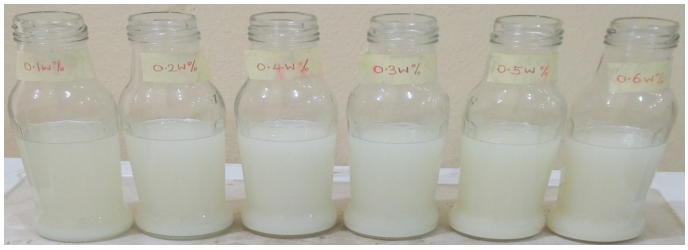

Figure 1. Prepared nanofluids.

a dipole without an external field. Boundary-surface polarisation is commonly present in heterogeneous insulating materials such as impregnated-paper insulation, hard-pressed boards and taped insulation used in electrical machines, and even at voids in solid homogeneous dielectrics. Such materials normally have a low value of relative permittivity [12]. The total polarisation is $P = NE\alpha$. The space-charge polarisation is very small and can be neglected:

$$P = NE\alpha = NE(\alpha_e + \alpha_i + \alpha_o) = NE\left(4\pi\varepsilon_0 R^3 + \frac{e^2}{\omega_0^2}\left(\frac{1}{m} + \frac{1}{M}\right) + \frac{\mu^2}{3k_B T}\right). \quad (9)$$

2.3. DIELECTRIC LOSS

Dielectric loss is defined as

$$\tan\delta = \frac{\varepsilon''}{\varepsilon'} = \frac{1}{\omega RC}, \quad (10)$$

where δ is the angle between the charging and active currents, called the loss angle. The loss tangent, $\tan\delta$, measures the inadequacy of dielectric constituents. Dielectric loss is influenced by both frequency and temperature. When temperature increases, ion mobility increases, further enhancing conduction through the polarisation process. Loss therefore increases with higher temperature. Viscosity describes the resistance of a fluid to flow, and dynamic viscosity measures this resistance when an external force is applied. The viscosity of insulating fluids plays a significant role in heat transfer and is highly temperature-dependent [13]. When the insulating fluid is heated, its molecules vibrate around their average positions, increasing their kinetic energy. The increase in average kinetic energy is linked to a decrease in the frictional force within the layers of the insulating fluid [14]. Temperature in transformers tends to rise continuously because of power losses from their windings and magnetic circuits [15]. As a result, insulating fluids are crucial for dissipating heat in liquid-filled power equipment. They help reduce component temperature to suitable levels and support reliable operation of oil-filled power systems [16].

Conductivity, σ, is also a function of the imaginary permittivity ε'', which describes energy loss:

$$\sigma = \frac{J_l}{E} = \omega\varepsilon'', \quad (11)$$

where J_l is the leakage-current density and E is the applied electric field.

The correlation between viscosity and temperature is analysed using an Arrhenius plot:

$$\eta = A\exp\left(\frac{E_a}{kT}\right), \quad (12)$$

where A is the pre-exponential term, η is viscosity, T is temperature in kelvin, k is the Boltzmann constant and E_a is the activation energy determined from the slope of a plot of $\ln(\eta)$ against $1/T$ [14]. Activation energy is the energy required to restrict the mobility of charge carriers contained in the fluid. Hence, a suitable insulating fluid has high activation energy.

3. SAMPLE PREPARATION AND METHODOLOGY

3.1. SAMPLE PREPARATION

The nanofluids were prepared by a two-step method, in which coated nanoparticles were dispersed into fatty acid methyl ester (FAME) and stirred at 800 rpm for 2 h [17]. This approach is preferred because of its affordability and practical ease during preparation [18]. Before measurements, suspended particles were separated from sediments. Highly purified methyl ester and nanofluid samples were prepared at different concentrations (wt%). Figure 1 shows the prepared nanofluids, and Figure 2 shows the sample-preparation process.

3.2. STABILITY OF NANOFLUIDS

The stability of the nanofluids was observed using the sedimentation method, in line with previous studies [19, 20]. The most stable nanofluid sample was considered to be the sample that retained more suspended nanoparticles over a long period. The suspension mass for each sample was determined 30 d after preparation. Functionalised and nonfunctionalised nanoparticles were dispersed into FAME at the same concentration of 0.6 wt%, and each sample was stirred for 3 h. After 30 d, the suspended nanoparticles were measured by decanting the nanofluid and leaving the sediment at the bottom of the beaker. The mass of the filter paper was measured and recorded. The sedimented nanoparticles were filtered, and the residue was washed with methanol, heated and dried in a vacuum oven at 40 °C for 30 min.

3.3. X-RAY DIFFRACTION AND SCANNING ELECTRON MICROSCOPY-ENERGY-DISPERSIVE X-RAY SPECTROSCOPY

The TiO_2 nanoparticles were characterised using an X-ray diffraction (XRD) Rigaku MiniFlex 300 system operating in reflection mode with copper radiation of wavelength $\lambda = 1.54059$ Å at 40 kV and 30 mA. Data were taken for the 2θ range of 5°–80°. The average crystallite size was calculated using the X-ray wavelength and the peak breadth, β, in radians through the Scherrer equation [21, 22]:

$$D = \frac{0.9\lambda}{\beta\cos\theta}. \quad (13)$$

3.4. MEASUREMENT OF VISCOSITY

The dynamic viscosity of the samples was measured using an RVDV-1 Brookfield digital viscometer according to ASTM D445, first at constant temperature and then at temperatures from

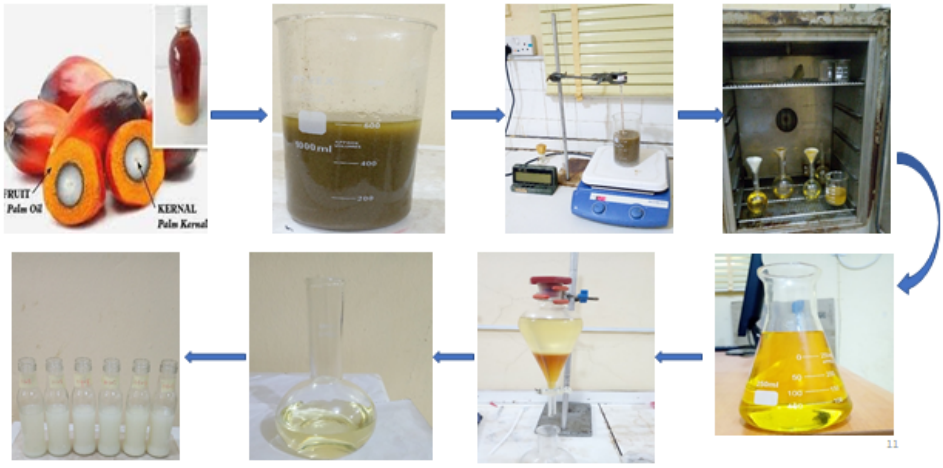

Figure 2. Preparation of samples.

Figure 3. Viscosity measurement setup.

30 to 80 °C at 10 °C intervals. The experimental setup is presented in Figure 3.

3.5. MEASUREMENT OF POUR POINT

The pour point of methyl ester (ME) and the nanofluids was measured according to ASTM D5949 (2022) [23]. The nanofluid was heated to 48 °C, after which the test jar was transferred to a bath maintained at 24 ± 1.5 °C. The specimen was cooled at a rate of 1.5 °C, and its flow characteristics were examined visually. The test jar was tilted at temperature intervals of 4 °C. The lowest temperature at which movement of the test specimen was visually observed was recorded as the pour point of the sample.

Figure 4. Rohde & Schwarz HM8118 programmable LCR bridge.

3.6. MEASUREMENT OF FLASH POINT

The flash point was determined experimentally by heating the liquid in a container and introducing a small flame just above the liquid surface. The lowest temperature at which there was a flash or ignition was recorded as the flash point according to ASTM D93.

3.7. RELATIVE PERMITTIVITY AND LOSS FACTOR

The relative permittivity and loss factor of the samples were measured according to IEC 60247:2004 using a Rohde & Schwarz HM8118 programmable LCR bridge. The measurement setup is shown in Figure 4.

3.8. DC LEAKAGE CURRENT AND BREAKDOWN STRENGTH

The test cell was filled with nanofluid containing homogenised nanoparticles. The electrode of the test cell was adjusted to 2.5 mm according to IEC 60156:2018. The test cell was then connected to a high-voltage source through a series current-limiting resistor of 1 MΩ. The voltage was slowly and cautiously increased stepwise at 1 kV s^{-1}, and the potential difference across the measuring resistor was measured using a benchtop digital multimeter until breakdown occurred. Five breakdowns were conducted for each sample, and the average value was taken. The leakage current was determined from the measured voltage

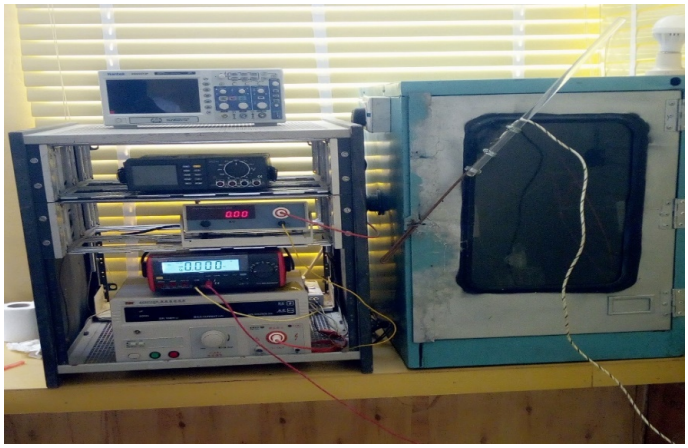

Figure 5. Dielectric-breakdown measurement setup.

Table 1. Sample codes used for stability identification.

Sample	Code
Uncoated nanofluid	UCNF
First coated nanofluid	1CNF
Second coated nanofluid	2CNF
Third coated nanofluid	3CNF
Fourth coated nanofluid	4CNF
Fifth coated nanofluid	5CNF
Sixth coated nanofluid	6CNF
Seventh coated nanofluid	7CNF
Eighth coated nanofluid	8CNF
Ninth coated nanofluid	9CNF
Tenth coated nanofluid	10CNF

across the measuring resistor and the resistance of the resistor using Ohm's law.

3.9. AC BREAKDOWN STRENGTH

The AC breakdown voltage of the samples was measured according to ASTM D1816 (2019). An automated insulating-oil dielectric-strength tester, model FS2080, was used to determine the dielectric breakdown of each oil sample. The electrodes of the test kit had a mushroom shape with a gap spacing of 2 mm. Approximately 250 mL of oil was used for each sample, and the breakdown-voltage test was carried out by increasing the supply voltage stepwise at 1 kV s^{-1} until breakdown occurred. For statistical analysis, five breakdown-voltage data points were taken. The measured average breakdown voltage and Weibull distribution were compared, and the characteristic breakdown voltage was determined. Figure 5 shows the dielectric-breakdown measurement setup.

4. RESULTS AND DISCUSSION

4.1. SAMPLE DESCRIPTION

Table 1 explains the sample codes used for stability identification. Table 2 explains the sample codes used for the dielectric tests and the percentage of suspended nanoparticles in them.

Table 2. Sample codes for dielectric tests and the corresponding suspended-nanoparticle percentages.

Sample	Code	Suspended nanoparticle (wt%)
Methyl ester	ME	0.00
Eighth coated nanoparticle at 0.1 wt%	ECNF0.1	0.037
Eighth coated nanoparticle at 0.2 wt%	ECNF0.2	0.07
Eighth coated nanoparticle at 0.3 wt%	ECNF0.3	0.11
Eighth coated nanoparticle at 0.4 wt%	ECNF0.4	0.15
Eighth coated nanoparticle at 0.5 wt%	ECNF0.5	0.18
Eighth coated nanoparticle at 0.6 wt%	ECNF0.6	0.22

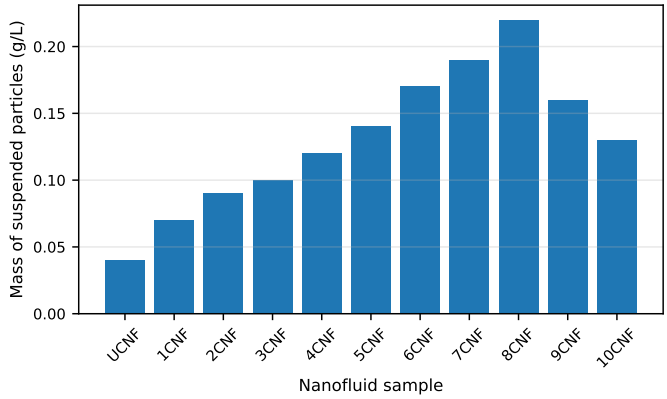

Figure 6. Variation in suspended nanoparticles in nanofluid samples.

4.2. STABILITY OF NANOFLUIDS

Nanoparticles agglomerate when dispersed in ME because they have small surface area and very high surface energy [24]. The UCNF sample had 0.04 g L^{-1} of suspended mass and showed more sedimentation owing to the lack of surfactant. Hence, coating or surface modification improves the stability of nanofluids [25, 26]. The presence of surfactant in the nanofluids reduced sedimentation and agglomeration of the nanoparticles [27]. The suspended quantity for all samples at 0.6 wt% is shown in Figure 6.

The 1CNF, 2CNF, 3CNF, 4CNF, 5CNF, 6CNF, 7CNF, 8CNF, 9CNF and 10CNF samples had suspended masses of 0.07, 0.09, 0.10, 0.12, 0.14, 0.17, 0.19, 0.22, 0.16 and 0.13 g L^{-1}, respectively. The suspended mass increased with the number of coatings up to a certain value, and the 8CNF sample displayed the optimum stability performance. Eight-times coated nanoparticles were therefore used to prepare nanofluids at varying concentrations of 0.1–0.6 wt%. The prepared samples were used for physical and dielectric-property measurements.

4.3. FOURIER-TRANSFORM INFRARED ANALYSIS

Fourier-transform infrared (FTIR) characterisation was performed using infrared absorption and vibration generated by the diverse functional groups to reveal the chemical composition of the samples [28]. The FTIR spectra of pure TiO_2 and oleic-acid-coated TiO_2 are shown in Figures 7 and 8, respectively. In Figure 7, the band at 3235 cm^{-1} is associated with symmetric and asymmetric stretching modes of hydroxyl groups (Ti–OH) [29, 30]. Furthermore, deformation vibration of the Ti–OH bending mode

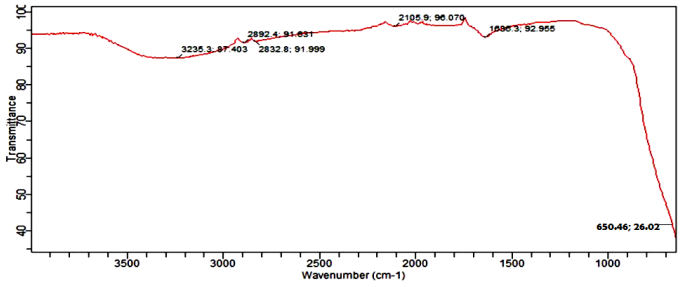

Figure 7. FTIR spectrum of pure TiO_2.

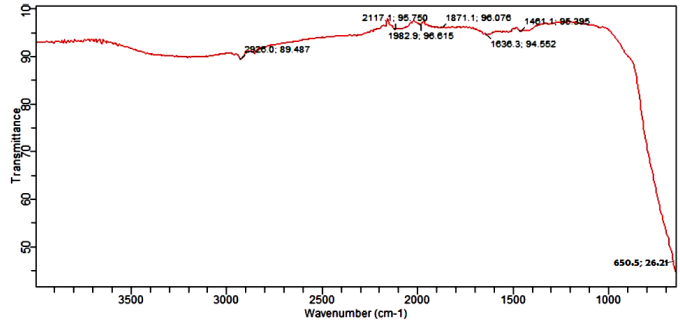

Figure 8. FTIR spectrum of oleic-acid-coated TiO_2.

was found at 1636 cm^{-1} [31]. The two detected peaks correspond to O–H bending modes of adsorbed water and hydroxyl groups on the TiO_2 surface. The band from 1000 to 400 cm^{-1} has been identified in the literature as the fingerprint of Ti–O stretching and Ti–O–Ti bridging stretching modes [32]. The peak at 650 cm^{-1}, which is within the anatase titania range, indicates that the TiO_2 nanoparticles used were anatase [33].

In Figure 8, the oleic-acid-coated TiO_2 nanoparticle shows a strong CH_2 absorption peak at 2926 cm^{-1} that is not present in pure TiO_2, reflecting the presence of oleic acid in the coated TiO_2 used for surface coating. The peak at 1461 cm^{-1} indicates carboxylate and demonstrates the interaction of oleic acid and nanoparticle surfaces through physical and chemical bonding. The carboxylate peak reveals the reaction between the –COOH group of oleic acid and the –OH group of TiO_2 nanoparticles. These findings are in good agreement with those presented by Zou et al. [34].

4.4. X-RAY DIFFRACTION ANALYSIS

The powder XRD pattern of the TiO_2 nanoparticles was used to determine the average crystallite size. In Figure 9, the diffraction peaks are attributable to TiO_2, and the two intense peaks at 2θ = 25.26° and 47.84° can be indexed to the anatase phase (JCPDS file No. 21-1272). The XRD pattern of TiO_2 is also in good agreement with results reported in the literature [35, 36]. The mean crystallite size of the nanoparticles was calculated using Eq. (13). The average particle sizes of TiO_2 were 11 and 18 nm.

4.5. VISCOSITY

According to IEC 60296:2020, the maximum viscosity of insulating fluid is 12 mPa s at a reference temperature of 40 °C. As shown in Figure 10, the viscosity of the samples increased with

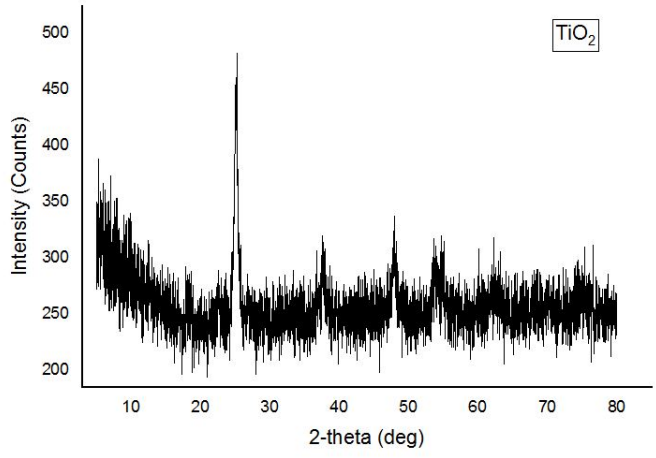

Figure 9. XRD spectrum of TiO_2 nanoparticles.

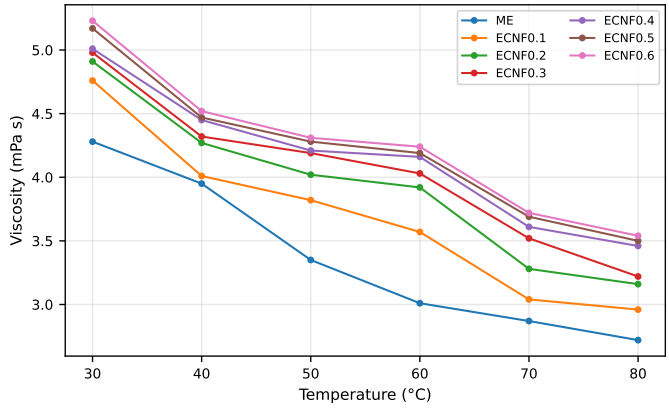

Figure 10. Variation of viscosity with sample temperature.

increasing loading at the same temperature. At 40 °C, the percentage increase in viscosity from ME to ECNF0.1 was modest, with values of 3.95 and 4.01 mPa s, respectively, compared with the increase from ECNF0.1 to ECNF0.2. Similar patterns were found in the remaining samples. This variation could be due to intermolecular forces affected by an increase in nanoparticle loading. The viscosities of ECNF0.5 and ECNF0.6 were 4.47 and 4.52 mPa s, respectively. Figure 10 also shows that increasing temperature caused a decrease in the viscosity of all samples. This is because heat increases each molecule's thermal or kinetic energy. As a result, the cohesive energy of the molecules reduces the resistive force acting between the layers of liquid molecules. This enhances molecular mobility, reducing viscosity [13]. The results showed that coating had no significant effect on viscosity and confirmed that the nanofluid meets the requirements for insulating oil.

The viscosity measurements were plotted against temperature to produce an Arrhenius plot (Figure 11). The activation energy of each sample was calculated from the slope of the Arrhenius plots, as shown in Table 3. As indicated in the table, activation energy increased by dissociating the molecules, preventing a rapid rise in particle-charge mobility in the fluids and reducing conduction by limiting ion mobility. A good insulat-

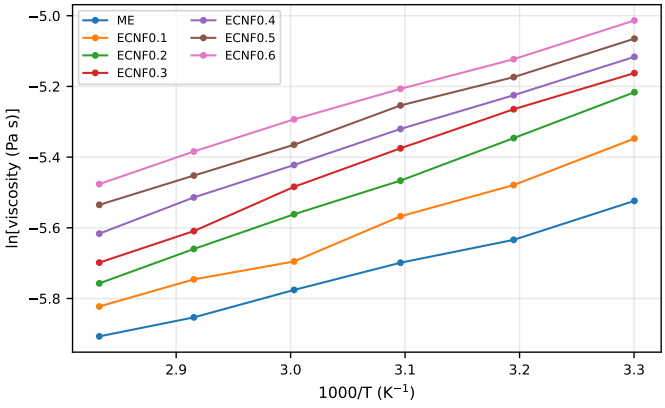

Figure 11. Arrhenius plot for sample viscosity.

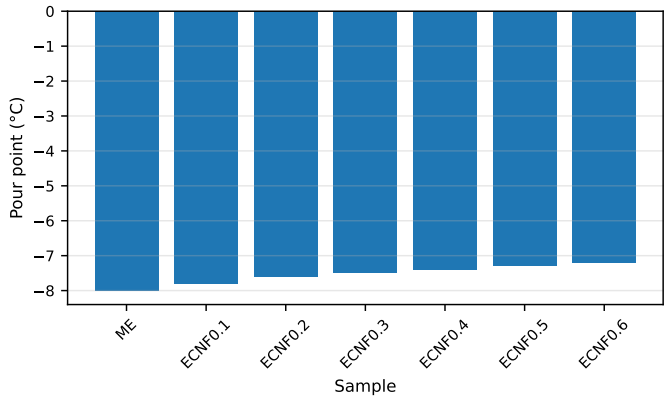

Figure 12. Pour point of the samples.

Table 3. Activation energy of the samples.

Sample	Activation energy (eV mol^{-1})
ME	0.07
ECNF0.1	0.08
ECNF0.2	0.09
ECNF0.3	0.10
ECNF0.4	0.12
ECNF0.5	0.13
ECNF0.6	0.14

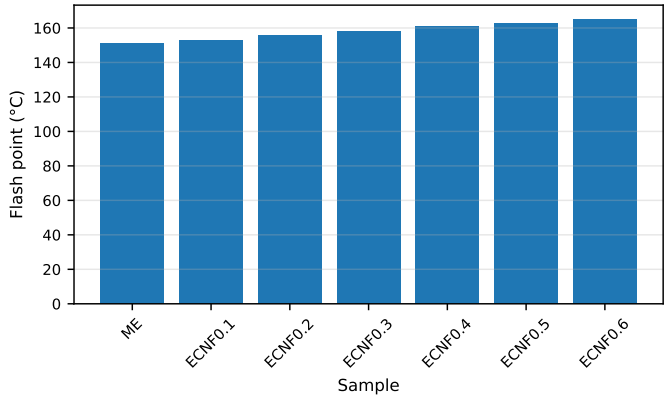

Figure 13. Flash point of the samples.

ing fluid must have high activation energy, low conductivity and low viscosity. The higher the activation energy, the more energy is required to reduce the nanofluid viscosity. The activation energy increased with concentration by lowering charge mobility [37, 38]. Thus, adding coated nanoparticles to oil had little influence on viscosity but improved the dielectric characteristics.

4.6. MEASUREMENT OF POUR POINT

Good insulating fluids are expected to flow under severely cold conditions to dissipate heat in power equipment during operation and to serve as cooling agents that prevent system damage. The pour points of ME and the nanofluid were measured using ASTM D5949 [23]. The pour points of purified palm kernel oil (PPKO) and natural ester were determined to be 25 and −4 °C, respectively. The substantial decrease in the pour point of PPKO can be attributed to the removal of glycerol, the viscous component of the oil. The elimination of glycerol lowered the number of O–H hydrogen bonds. This reduced the average molecular mass of the oil and the ability of the fatty acid chains to entangle, reducing the melting temperature of the ester to −4 °C [13], which is twice the value of −8 °C reported in this study. As shown in Figure 12, the pour point of the nanofluids increased with concentration. This could be attributed to the influx of oxygen molecules from TiO_2 nanoparticles, which oxidised ME and increased the oil pour point. According to IEC 60247, liquid dielectric has a maximum pour point of −45 °C. Therefore, multiple coatings did not pose problems for the pour point.

4.7. MEASUREMENT OF FLASH POINT

The higher the flash point of insulating fluids, the more thermally stable they are. Increasing the flash point of the samples therefore improves their performance. The minimum flash point required according to IEC 60296 is 135 °C. ME had a flash point of 151 °C, which is higher than the 148 °C reported in previous studies [13]. This could be related to a reduction in the glycerol level in the oil. Figure 13 shows the flash points of all samples. The results show that adding coated nanoparticles at increasing concentrations increased the flash point of the insulating fluids. This could be related to the lack of particle-charge mobility, which reduces conduction and enables the oil molecules to dissociate more easily. The findings indicate that adding coated nanoparticles to the base oil improves the dielectric properties relevant to power equipment.

4.8. RELATIVE PERMITTIVITY

Figure 14 illustrates the relative permittivity calculated by dividing the sample capacitance by the capacitance of free space. It can be concluded that permittivity is slightly frequency-dependent. Permittivity decreased slightly as frequency increased because permittivity is a function of capacitance. Insulating fluid that serves as a good coolant has higher permittivity because capacitance determines the energy-storage capability of the oil. The permittivity of ME was approximately 3.24,

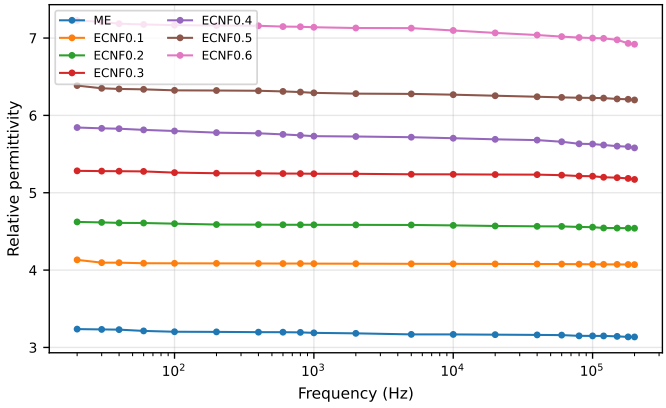

Figure 14. Permittivity as a function of sample frequency.

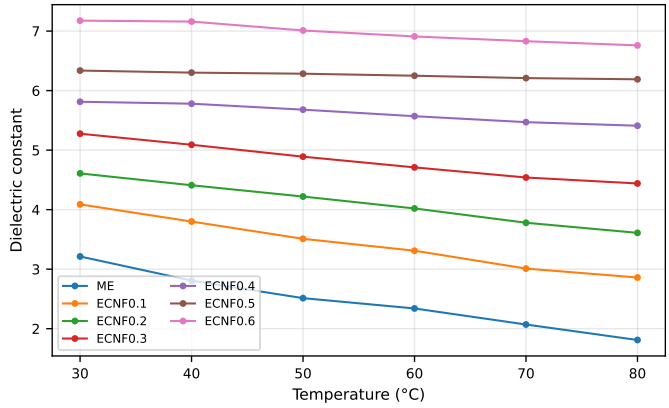

Figure 15. Permittivity as a function of temperature.

which is nearly identical to the value found by Oparanti et al. [38]. Researchers have further shown that the overall polarisation can be calculated as the sum of base-oil polarisation, internal polarisation of nanoparticles and orientation polarisation of charged nanoparticles as polar molecules [37]. Dielectric insulating fluids with high dielectric constants are used in distribution and power transformers [10]. The dielectric-constant values of the nanofluids were compared with those of transformer mineral oil, and the results suggest that nanofluids with higher dielectric-constant values can be used to insulate oil-filled power equipment. Owing to increased nanoparticle concentration, the nanofluid had higher permittivity than ME. The results showed that as nanoparticle concentration increased, permittivity also increased because the nanoparticles trapped and detrapped charged particles in the oil. In addition, because charged particles have mass and inertia, polarisation is expected to decrease as frequency increases. This leads to the conclusion that surface modification has no significant effect on permittivity, whereas the addition of nanoparticles enhances oil permittivity.

4.9. PERMITTIVITY WITH TEMPERATURE VARIATION

Figure 15 shows the dielectric constant of samples at temperatures from 30 to 80 °C at 10 °C intervals. The dielectric constants of all samples followed the same pattern and decreased as temperature increased. ME had lower dielectric-constant values than the nanofluid samples, with values of 3.21 at 30 °C and 1.81 at 80 °C. This is comparable to the findings of Hamid et al. [39], who reported that the dielectric constant of canola oil was 2.005 at 30 °C and decreased to 1.863 at 90 °C. The dielectric constant decreases with increasing temperature because of weaker interactions between molecules [10]. The increase in temperature also increases the kinetic energy of the insulating-fluid molecules, resulting in more random motion and reducing dipole orientation, thereby reducing the dielectric constant.

4.10. DIELECTRIC LOSS FACTOR

Figure 16 presents the frequency dependence of dielectric loss. Dielectric loss decreased with increasing frequency, in agreement with Eq. (10). As the concentration of TiO_2 nanoparticles increased, the dielectric loss decreased. This is because nanoparticles capture and release free-moving electrons, or streamers

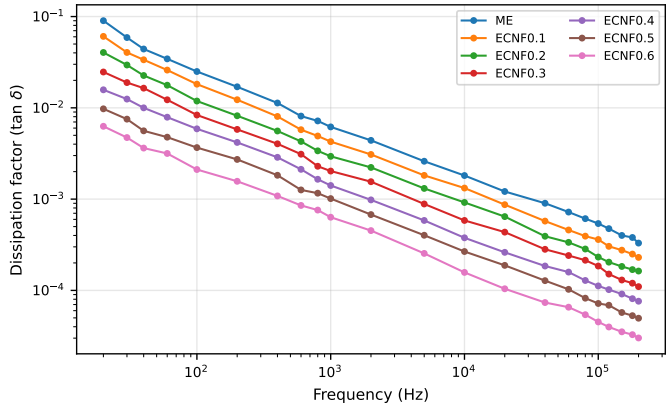

Figure 16. Dielectric loss of the samples as a function of frequency.

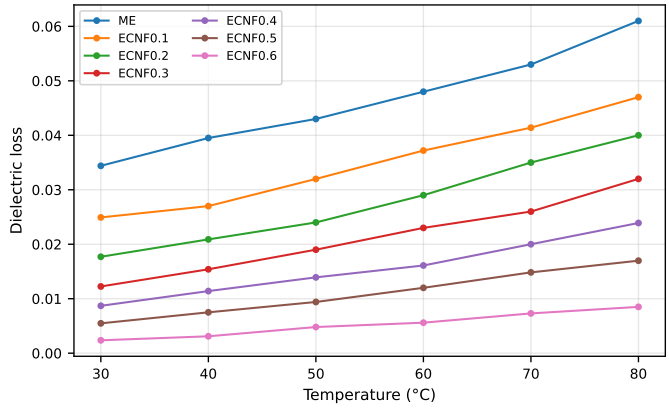

Figure 17. Comparison of dielectric loss with temperature.

[40]. This reduces the kinetic energy of fast-moving electrons and lowers the conduction rate of the insulating fluids. Conduction is directly proportional to dielectric loss, as shown in Eq. (11). Therefore, the electric charges responsible for conduction were captured by the nanoparticles, leading to a reduction in the loss tangent [41].

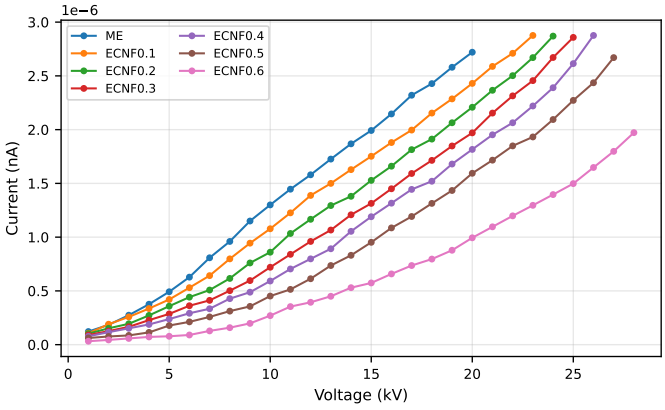

Figure 18. Current–voltage curves of the samples.

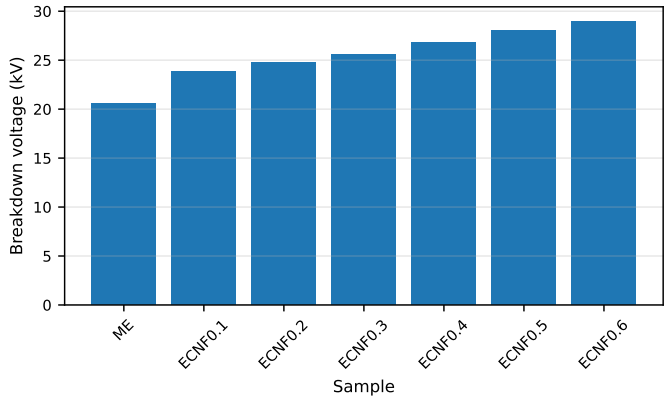

Figure 19. DC breakdown voltages of the samples (d = 2.5 mm).

4.11. DIELECTRIC LOSS WITH TEMPERATURE VARIATION

Figure 17 shows the variation in dielectric loss with temperature. As temperature increased, dielectric loss gradually increased. The increase in dielectric loss could be attributed to the increase in average kinetic energy of the molecules in the nanofluids, which causes charges to vibrate rapidly about their mean position. This vibration increases ionic conduction in the fluids.

4.12. HIGH-VOLTAGE DC BREAKDOWN ANALYSIS

Figure 18 shows the current–voltage curves of the samples, demonstrating the behaviour of leakage current, or conduction current, as voltage increased. Because of the non-Ohmic nature of the capacitor, leakage current increased symmetrically rather than linearly with voltage. The data also show that as nanoparticle loading increased, leakage current decreased. This could be due to charge-carrier trapping through polarisation and charge-induction mechanisms, which enhance insulating properties [42].

The measured dielectric breakdown voltage (BDV) for all samples is shown in Figure 19. Dielectric breakdown increased with nanoparticle concentration. This is due to a decrease in the effective width of double layers, which reduces interparticle distance. Nanoparticles can be readily ionised by generating an electric field, bridging the electron flow [43]. Makmud et al. [37] predicted that the breakdown of liquid dielectric will eventually increase.

4.13. WEIBULL STATISTICAL AC BREAKDOWN

Figures 20–22 show the Weibull graphs for all prepared samples. The statistical analysis followed standard guidance for electrical-insulation breakdown data [44]. The characteristic breakdown voltage increased as nanoparticles were dispersed in the base fluid. Figure 20 shows the Weibull plots for ME and ECNF0.1. The slopes of the two samples are substantially identical, indicating a close β parameter. The β parameter of ME falls within the range reported by Abdelmalik et al. [13]. ECNF0.1 had a larger β parameter and characteristic breakdown value than ME. The low value of the β shape parameter of ME suggests that the breakdown data are concentrated around a modal point. ECNF0.3 had a greater characteristic breakdown value than ECNF0.2 (Figure 21). Figure 22 shows the Weibull charts for ECNF0.4, ECNF0.5

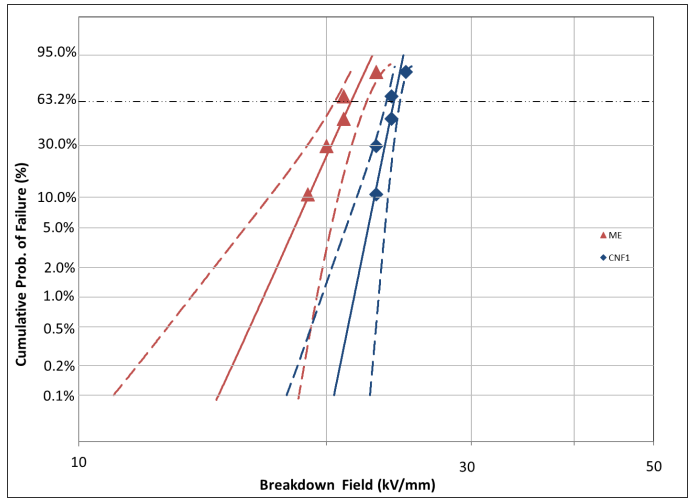

Figure 20. Two-parameter Weibull plot of AC breakdown voltage for ME and ECNF0.1.

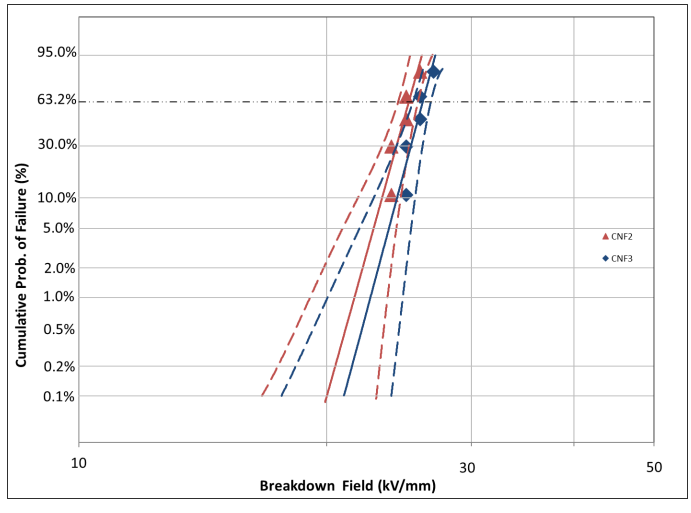

Figure 21. Two-parameter Weibull plot for ECNF0.2 and ECNF0.3.

and ECNF0.6. The dielectric breakdown rate increased with the concentration of dispersed TiO_2 nanoparticles. ECNF0.6, which contained 0.22 wt% dispersed nanoparticles, increased the characteristic breakdown strength of the nanofluid. This was due to

Table 4. Shape parameter, scale parameter and correlation coefficient obtained from two-parameter Weibull plots.

Sample	N	Characteristic breakdown strength, α (kV mm^{-1})	95% confidence bound for α (kV mm^{-1})	Shape parameter, β	95% confidence bound for β	ρ correlation coefficient
ME	5	21.4	18.50–23.94	18.63	10.61–44.70	0.956
ECNF0.1	5	24.2	21.99–25.96	28.94	16.48–69.42	0.907
ECNF0.2	5	25.2	22.99–26.96	30.14	17.16–72.32	0.907
ECNF0.3	5	26.2	23.98–27.96	31.35	17.85–75.21	0.906
ECNF0.4	5	27.2	24.98–28.96	32.56	18.54–78.11	0.906
ECNF0.5	5	28.3	26.67–29.59	46.21	26.31–110.86	0.919
ECNF0.6	5	29.3	27.67–30.59	47.85	27.25–114.80	0.919

Table 5. Weibull probability of the AC breakdown voltage for all samples.

Weibull probability (%)	ME	ECNF0.1	ECNF0.2	ECNF0.3	ECNF0.4	ECNF0.5	ECNF0.6
1	16.75	20.63	21.62	22.61	23.60	25.62	26.62
5	18.29	21.83	22.82	23.82	24.82	26.54	27.54
10	19.01	22.38	23.37	24.37	25.37	26.96	27.96
30	20.29	23.34	24.34	25.34	26.34	27.68	28.68
63.2	21.45	24.19	25.19	26.19	29.19	28.31	29.31

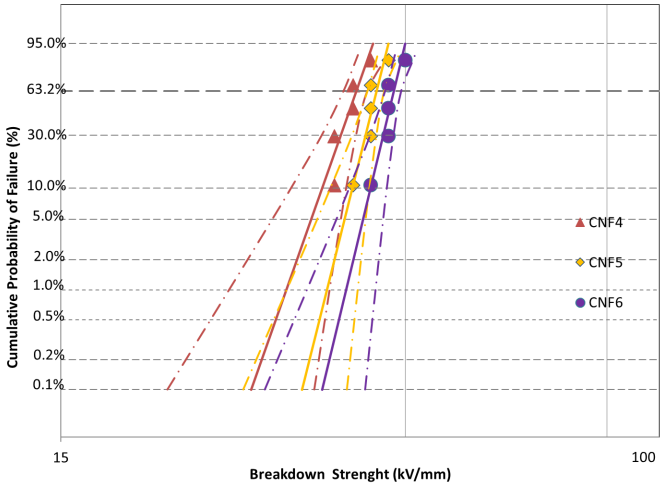

Figure 22. Two-parameter Weibull plot for ECNF0.4, ECNF0.5 and ECNF0.6.

a reduction in interparticle distance and the possible breadth of the double layers. This may have resulted in nanoparticle overlap, which, under a high electric field, may become ionised and bridge the flow of electrons.

The Weibull parameters and their 95% confidence intervals are summarised in Table 4.

It can be observed from Table 4 that the correlation coefficients of the breakdown data, when fitted in the Weibull function, are close to 1, indicating a strong positive correlation between Weibull probability and AC breakdown strength for the samples. The low values of the shape parameter for all samples indicate that the breakdown data are clustered around a modal point for all samples.

Table 5 presents the Weibull probability of the AC breakdown voltage for all samples.

It was observed that, at each probability level, the AC breakdown voltage of all nanofluid samples was better than that of ME (Table 5). The addition of TiO_2 nanoparticles to the ester helped to reduce electron transport in the nanofluid through repeated trapping and detrapping with the aid of shallow traps. These traps convert fast electrons created by the high electric field to slow electrons through the hopping process. The dielectric strength of the oil was increased through this hopping process by reducing the speed of the electrons and preventing the accumulation of space charges in the oil.

5. CONCLUSION AND RECOMMENDATIONS

Based on the investigation and the analysis of the results, multiple surface modifications of TiO_2 nanoparticles had no significant effect on dielectric properties but increased the stability of the nanofluids. Optimum nanofluid stability was achieved after eight coating cycles. In addition, the insulating properties of all samples improved with increasing concentration of eight-times coated nanoparticles in the ester-based oil. ECNF0.6 was therefore found to be the best insulating material among the tested samples for use in oil-filled power equipment for cooling and insulation. Surface modification increased nanofluid stability, and the addition of nanoparticles to ester oil improved dielectric performance.

On the basis of the results obtained in this study, the following recommendations are made. Although surface modification improves stability over time, further studies are required to improve stability for longer periods, because transformers are operated for very long durations and longer maintenance intervals are desirable. Although the nanofluid produced was stable for an extended period using sedimentation and centrifugation methods, further research should use other methods to identify the best alternative method for enhancing the stability of dispersed nanoparticles. In this study, the highest amount of coated TiO_2 dispersed into ME was 0.6 wt%. Therefore, the optimum breakdown-voltage performance was not observed, and further study above this value using eight-times coated TiO_2 nanoparticles is recommended.

DATA AVAILABILITY

The data will be available on request from the corresponding author.

References

[1] S. U. S. Choi, ''Enhancing thermal conductivity of fluids with nanoparticles'', ASME International Mechanical Engineering Congress and Exposition **17421** (1995) 99. https://doi.org/10.1115/IMECE1995-0926.

[2] J. A. Eastman, S. U. S. Choi, S. Li, W. Yu & L. J. Thompson, ''Anomalously increased effective thermal conductivities of ethylene glycol-based nanofluids containing copper nanoparticles'', Applied Physics Letters **78** (2001) 718. https://doi.org/10.1063/1.1341218.

[3] C. W. Nan, G. Liu, Y. Lin & M. Li, ''Interface effect on thermal conductivity of carbon nanotube composites'', Applied Physics Letters **85** (2004) 3549. https://doi.org/10.1063/1.1808874.

[4] L. Wang, W. Ma, L. Xu, W. Chen, Y. Zhu, C. Xu & N. A. Kotov, ''Nanoparticle-based environmental sensors'', Materials Science and Engineering: R: Reports **70** (2010) 265. https://doi.org/10.1016/j.mser.2010.06.012.

[5] P. Keblinski, S. R. Phillpot, S. U. S. Choi & J. A. Eastman, ''Mechanisms of heat flow in suspensions of nano-sized particles (nanofluids)'', International Journal of Heat and Mass Transfer **45** (2002) 855. https://doi.org/10.1016/S0017-9310(01)00175-2.

[6] L. S. Freitas, ''Preparation and stability of TiO_2 nanoparticle suspensions in mineral oil for electric insulation applications'', Journal of Electrostatics **70** (2012) 439. https://doi.10.1201_9781003093527_previewpdf.pdf.

[7] A. Ghadimi, R. Saidur & H. S. C. Metselaar, ''A review of nanofluid stability properties and characterization in stationary conditions'', International Journal of Heat and Mass Transfer **54** (2011) 4051. https://doi.org/10.1016/j.ijheatmasstransfer.2011.04.014.

[8] R. Saini, ''A review on dielectric properties of mineral oil-based nanofluids and their applications'', Renewable and Sustainable Energy Reviews **16** (2012) 1308. https://doi:10.1109/ACCESS.2025.3597740.

[9] O. V. Tereshchenko, F. J. K. Buesink & F. B. J. Leferink, ''An overview of the techniques for measuring the dielectric properties of materials'', General Assembly and Scientific Symposium (2011) 1. https://doi.org/10.1109/URSIGASS.2011.6050287.

[10] Z. H. Shah & Q. A. Tahir, ''Dielectric properties of vegetable oils'', Journal of Scientific Research **3** (2011) 481. https://doi.org/10.3329/jsr.v3i3.7049.

[11] T. Toudja, H. Moulai & A. Nacer, ''Moisture and electrical discharges effect on naphthenic mineral oil properties'', IET Science, Measurement & Technology **8** (2014) 588. https://doi.org/10.1049/iet-smt.2013.0262.

[12] R. Arora & W. Mosch, *High Voltage and Electrical Insulation Engineering*, John Wiley & Sons, 2011. https://sisis.rz.htw-berlin.de/inh2012/12429346.pdf.

[13] A. A. Abdelmalik, ''The feasibility of using a vegetable oil-based fluid as electrical insulating oil'', PhD Thesis, Department of Engineering, University of Leicester, 2012. https://hdl.handle.net/2381/10374.

[14] S. A. Umar, A. A. Abdelmalik & A. N. Nura, ''Synthesis and characterization of a potential bio-based dielectric fluid from neem oil seed'', Industrial Crops and Products **115** (2018) 117. https://doi.org/10.1016/j.indcrop.2018.02.009.

[15] S. V. Kulkarni & S. A. Khaparde, *Transformer Engineering: Design and Practice*, 1st ed, CRC Press, Boca Raton, United States, 2004, 469. https://doi.org/10.1201/9780367800598.

[16] M. S. Mohamad, H. Zainuddin, S. A. Ghani, I. S. Chairul & A. A. Abdelmalik, ''AC breakdown voltage and viscosity of palm fatty acid ester (PFAE) oil-based nanofluids'', Journal of Electrical Engineering & Technology **12** (2017) 2333. https://www.researchgate.net/publication/320621325_AC_Breakdown_Voltage_and_Viscosity_of_Palm_Fatty_Acid_Ester_PFAE_Oil-based_Nanofluids.

[17] J. Jacob, P. Preetha & S. R. G. Nair, ''Review on natural ester and nanofluids as an environmental friendly alternative to transformer mineral oil'', IET Nanodielectrics, Montpellier, France, **3** (2020) 33. https://doi.org/10.1049/iet-nde.2019.0038.

[18] V. Primo, A. García, B. García & J. C. Burgos, ''Applicability of nanodielectric fluids to the improvement of transformer insulation properties'', IEEE International Conference on Dielectrics **1** (2016) 76. https://doi.org/10.1109/ICD.2016.7547547.

[19] X. Wei & L. Wang, ''Synthesis and thermal conductivity of microfluidic copper nanofluids'', Particuology **8** (2010) 262. https://doi.org/10.1016/j.partic.2010.03.001.

[20] X. Li, D. Zhu & X. Wang, ''Evaluation on dispersion behavior of the aqueous copper nano-suspensions'', Journal of Colloid and Interface Science **310** (2007) 456. https://doi.org/10.1016/j.jcis.2007.02.067.

[21] A. Guinier, *X-ray Diffraction in Crystals, Imperfect Crystals, and Amorphous Bodies*, Courier Corporation, 1994. https://cir.nii.ac.jp/crid/1571135649249351936.

[22] D. O. Obada, E. T. Dauda, J. K. Abifarin, D. Dodoo-Arhin & N. D. Bansod, ''Mechanical properties of natural hydroxyapatite using low cold compaction pressure: Effect of sintering temperature'', Materials Chemistry and Physics **239** (2020) 122099. https://doi.org/10.1016/j.matchemphys.2019.122099.

[23] L. V. Sani, V. O. Ajibola & S. E. Abechi, ''Production and characterization of biodiesel-diesel blends from Terminalia catappa seed oil'', FUDMA Journal of Sciences **2** (2023) 214. https://fjs.fudutsinma.edu.ng/index.php/fjs/article/view/1339.

[24] B. Du & J. Li, ''Influence of monodisperse Fe_3O_4 nanoparticle size on electrical properties of vegetable oil-based nanofluids'', Journal of Nanomaterials **2015** (2015) 560352. https://doi.org/10.1155/2015/560352.

[25] M. V. Avdeev, T. V. Tropin, H. Aksenov, V. L. Aksenov, M. V. Rosta, V. M. Garamus & R. Willumeit, ''On the magnetic structure of magnetite/oleic acid/benzene ferrofluids by small-angle neutron scattering'', Journal of Magnetism and Magnetic Materials **270** (2004) 371. https://doi.org/10.1016/j.jmmm.2003.08.032.

[26] Y. Li, S. Tung, E. Schneider & S. Xi, ''A review on development of nanofluid preparation and characterization'', Powder Technology **196** (2009) 89. https://doi.org/10.1016/j.powtec.2009.07.025.

[27] W. Yu & H. Xie, ''A review on nanofluids: Preparation, stability mechanisms, and applications'', Journal of Nanomaterials **2012** (2012) 435873. https://doi.org/10.1155/2012/435873.

[28] R.-J. Liao, C.-J. Sun, J. Li & S. Grzybowski, ''Thermal aging microscale analysis of power transformer pressboard'', IEEE Transactions on Dielectrics and Electrical Insulation **15** (2008) 1281. https://doi.org/10.1109/TDEI.2008.4656235.

[29] P. Praveen, G. Viruthagiri, S. Mugundan & N. Shanmugam, ''Structural, optical and morphological analyses of pristine titanium dioxide nanoparticles synthesized via sol-gel route'', Spectrochimica Acta Part A: Molecular and Biomolecular Spectroscopy **117** (2014) 622. https://doi.org/10.1016/j.saa.2013.09.037.

[30] J. Abifarin, D. Dodoo-Arhin, F. A. Choysia, A. J. H. Kekani, D. O. Obada & A. A. Oyedeji, ''Experimental data on the characterization of hydroxyapatite synthesized from biowastes'', Data in Brief **26** (2019) 104485. https://doi.org/10.1016/j.dib.2019.104485.

[31] L. Chougala, M. Yatnatti, R. Linganagoudar, R. Kamble & J. Kadadevaramath, ''A simple approach on synthesis of TiO_2 nanoparticles and its application in dye sensitized solar cells'', Journal of Nano- and Electronic Physics **9** (2017) 04005. https://doi.org/10.21272/jnep.9(4).04005.

[32] H. Lu, Y. Zhou, S. Vongehr, S. Tang & X. Meng, ''Effects of hydrothermal temperature on formation and decoloration characteristics of anatase TiO_2 nanoparticles'', Science China Technological Sciences **55** (2012) 894. https://doi.org/10.1007/s11431-011-4706-4.

[33] X. Lu, X. Zhao & C. Wang, ''Nanocomposites of poly(L-lactide) and surface-grafted TiO_2 nanoparticles: Synthesis and characterization'', European Polymer Journal **44** (2008) 2476. https://doi.org/10.1016/j.eurpolymj.2008.06.002.

[34] P. Zou, J.-X. Zhang, T.-J. Guo & X. Li, ''Dielectric properties and electrodynamic process of natural ester-based insulating nanofluid'', Modern Physics Letters B **25** (2011) 2021. https://doi.org/10.1142/S0217984911027285.

[35] G. Rajakumar, A. A. Rahuman, S. M. Roopan, V. G. Khanna, G. Elango, C. Kamaraj & K. Velayutham, ''Fungus-mediated biosynthesis and characterization of TiO_2 nanoparticles and their activity against pathogenic bacteria'', Spectrochimica Acta Part A: Molecular and Biomolecular Spectroscopy **91** (2012) 23. https://doi.org/10.1016/j.saa.2012.01.011.

[36] T. Theivasanthi & M. Alagar, ''Titanium dioxide (TiO_2) nanoparticles XRD analyses: An insight'', arXiv preprint (2013) arXiv:1307.1091. https://doi.org/10.48550/arXiv.1307.1091.

[37] M. Z. H. Makmud, H. A. Illias, C. Y. Chee & M. S. Sarjadi, ''Influence of conductive and semi-conductive nanoparticles on the dielectric response of natural ester-based nanofluid insulation'', Energies **11** (2018) 333. https://doi.org/10.3390/en11020333.

[38] S. A. Oparanti, A. A. Abdelmalik & A. D. Usman, ''AC breakdown analysis of synthesized nanofluids for transformer insulation'', Research Square preprint (2021). https://doi.org/10.21203/rs.3.rs-453749/v1.

[39] M. H. Hamid, M. T. Ishak, M. F. M. Din, N. S. Suhaimi, N. A. Katim & N. Azis, ''Dielectric properties of natural ester oils used for transformer application under temperature variation'', IEEE International Conference on Power and Energy (2016) 54. https://doi.org/10.1109/PECON.2016.7951472.

[40] A. Katiyar, P. Dhar, T. Nandi, L. S. Maganti & S. K. Das, ''Enhanced breakdown performance of anatase and rutile titania based nano-oils'', IEEE Transactions on Dielectrics and Electrical Insulation **23** (2016) 3494. https://doi.org/10.1109/TDEI.2016.005886.

[41] Y. Zhang & Z. Wang, ''Measurement of dielectric loss tangent at cryogenic temperature using superconducting film resonator'', Journal of Theoretical and Applied Physics **10** (2016) 27. https://doi.org/10.1007/s40094-015-0197-1.

[42] J. G. Hwang, M. Zahn, F. M. O'Sullivan, L. A. A. Pettersson, O. Hjortstam & R. Liu, ''Effects of nanoparticle charging on streamer development in transformer oil-based nanofluids'', Journal of Applied Physics **107** (2010) 014310. https://doi.org/10.1063/1.3267474.

[43] M. E. Ibrahim, A. M. Abd-Elhady & M. A. Izzularab, ''Effect of nanoparticles on transformer oil breakdown strength: experiment and theory'', IET Science, Measurement & Technology **10** (2016) 839. https://doi.org/10.1049/iet-smt.2016.0104.

[44] G. C. Montanari, J. C. Fothergill, N. Hampton, R. Ross & G. Stone, *IEEE guide for the statistical analysis of electrical insulation breakdown data*, IEEE Standard 930-2004, 2005. https://standards.ieee.org/standard/930-2004.html.